Article

Stability Assessment of Tunnels Excavated in Loess with the Presence of Groundwater—A Case Study

Qihua Deng [1,2], **Junru Zhang** [3], **Feng Lu** [4], **Ziyan Fan** [3,*], **Yi Wang** [4,*] and **Zhi Lin** [5]

1   Faculty of Architecture, Civil and Transportation Engineering, Beijing University of Technology, Beijing 100124, China; dqh18635489278@163.com
2   China Railway 22 Bureau Group Co., Ltd., Beijing 100043, China
3   School of Civil Engineering, Southwest Jiaotong University, Chengdu 610031, China; jrzh@swjtu.edu.cn
4   School of Emergency Management, Xihua University, Chengdu 610039, China; fenglu0901@foxmail.com
5   College of Civil Engineering, Chongqing Jiaotong University, Chongqing 400074, China; zhilin@cqjtu.edu.cn
*   Correspondence: f75988@my.swjtu.edu.cn (Z.F.); wangyi7@stu.xhu.edu.cn (Y.W.)

Abstract: The high water content of the surrounding rock in loess tunnels will lead to the deterioration of rock strength, causing deformation and damage to the initial support structure and thereby affecting safety during construction and operation. This article first analyzes the strength characteristics of loess under different water contents through indoor physical and mechanical tests. Secondly, based on numerical simulation results, the ecological environment, and design requirements, the water content threshold is determined. Finally, a reinforcement scheme combining surface precipitation measures and curtain grouting measures is proposed, and the reinforcement effect is analyzed based on on-site monitoring data. The results show that as the water content of loess increases, the cohesion, internal friction angle, and elastic modulus of the surrounding rock all decrease, leading to an increase in the sensitivity of the surrounding rock to excavation disturbances and a deterioration in strength. During the construction process, it shows an increase in the vault settlement and sidewalls' convergence. During the process of increasing the distance between the monitoring section and the palm face, the settlement and convergence of the tunnel show a rapid growth stage, slow growth stage, and stable stage. The water content threshold is determined to be 22%. The reinforcement scheme of combining surface precipitation measures with curtain grouting measures not only meets the requirements of the ecological environment but also makes the settlement and convergence values lower than the yellow warning deformation values required by the design.

Keywords: loess tunnel; water content; deformation law; monitoring measurement; countermeasures

1. Introduction

With the rapid development of tunnel engineering in China, it is inevitable to encounter complex and unfavorable geological strata during the construction process [1–5]. Among them, the loess strata, due to their obvious structure, high permeability, collapsibility, and vertical joint development [6–10], will face construction risks such as water leakage, large deformation, falling blocks, and collapse when constructing tunnels in this stratum [11–14]; especially, the collapsibility of loess often causes the sudden instability of the surrounding rock in a short period, leading to disasters [15–17]. In addition, the disaster characteristics of loess may also lead to the cracking of the lining structure, thereby affecting the safe operation of tunnel engineering in the later stage [18–21].

Most loess tunnels are subject to waterfall erosion, lateral erosion, and headward erosion [22,23] due to surface water infiltration or groundwater erosion during the construction process, which in turn results in the reduction in the strength of the surrounding rock [24,25], large deformations, and wet subsidence of the loess [26–28]; therefore, the mechanism of structural failure in loess tunnels under different water contents is the focus of research. In addition, in groundwater flow simulation, the input parameters are

uncertain [29] and certain methods are needed to predict the parameters [30]. As the water content continues to increase, it contributes to the formation of a saturated zone at the bottom plate, which in turn affects the overall displacement of the tunnel [31], and in severe cases will lead to tunnel collapse [32]. Hong [33] conducted extensive literature research and found that the types of collapse and failure in loess tunnels can be divided into four types. Among them, the collapse and failure caused by water-rich loess in loess tunnels account for about 90% of the total. At present, the research on the deformation of loess water content on tunnel structure can be explored in depth based on the results of experiments and numerical simulations, in addition to the way of literature research. Liu [34] used a multipoint independent loading test system for tunnel lining to analyze the deformation and cracking of the lining structure based on the degradation mechanism of the mechanical properties of loess surrounding rock under the action of surface water. It was found that the development order of cracks in the lining structure is Type I initial cracks, Type L intermediate cracks, and Type Y later cracks, and the types of cracks in the lining are mostly concentrated in Type L. Xue [35] obtained sample data through a numerical simulation analysis of loess tunnels and proposed a model for predicting the total deformation of loess tunnels in combination with the Bulletin of Engineering Geology and the Environment (BPNN). The prediction model was applied to five loess tunnel engineering examples, and the results showed that the model can accurately predict the total deformation of loess tunnels. Qiu [36], based on the indoor model test combined with a numerical simulation, studied the effect of pipe surge water on underground loess, and the results showed that the maximum contact pressure appeared in the location of the bottom of the arch, independent of the location of the water surge; after the occurrence of the water surge, the surrounding rock will form a cavity area, and the whole area seems to experience a conical distribution. Li [37] analyzed the stress state of the tunnel structure through on-site large-scale immersion tests, and the results showed that as the water content of the loess surrounding rock near the tunnel lining structure gradually increased, the inverted arch began to produce upward displacement, and there was significant sinking at the arch foot. Cui [38] used the model test to determine that the loess tunnel arch position should be reserved as part of the deformation, and the deformation needs to be 2–4 times the sidewall. In addition, some studies have shown that the closer the lining structure is to the loess-wetted area, the greater the growth of its bending moment, axial force, and stress. Shao [39] evaluated the collapsibility characteristics of loess by using sand well immersion tests; during the experiment, the settlement rate of loess went from slow to fast, then to slow, and finally tended to stabilize. The collapse deformation of unsaturated loess is sudden and controlled by the water content. Many scholars have focused their research on the influence of a single factor on the structure of loess tunnels due to changes in the water level, with little consideration given to factors such as the water content or the distance between the monitoring section and the tunnel face on the deformation mechanism of the initial support structure of the tunnel. Regarding controlling the deformation of loess tunnel structures, Wei [40] proposed using curtain grouting to control the deformation of tunnel structures. Hong [33] proposed a scheme for reinforcing soft loess through the use of a pipe roof, advanced small pipes, and grouting. Hong [11] proposed the use of segmented large pipe sheds with grouting to reinforce collapsed areas. The above reinforcement schemes are all directly applied in loess tunnels and have not taken into account the influence of water content thresholds; after the implementation of the disposal plan, not only did it not reflect the optimal effect of the reinforcement plan, but it also lacked environmental and economic benefits.

In summary, this article first comprehensively analyzes the influence of groundwater in rock strata on the mechanical properties of loess. Secondly, based on the numerical simulation results of tunnel excavations under the influence of groundwater in different rock strata, the deformation mechanism of the initial support structure is explored under the influence of two factors: the water content and the distance between the monitoring section and the palm face. The groundwater action in rock strata is simulated in numerical

calculations by controlling the water content of the surrounding rock. Finally, a recommended threshold value for controlling the water content and corresponding measures for controlling tunnel structural deformation are proposed, reducing environmental damage and the construction safety risks caused by excessive water blocking or precipitation. The research results have good theoretical significance and application value for controlling the water content and deformation of the surrounding rock of loess tunnels and optimizing construction technology measures.

2. Project Overview

The Shangge Village Tunnel of the Yinxi High-Speed Railway (the Ganning Section) has a total length of 6782.45 m (DK 207 + 517.55-DK 214 + 300), with a burial depth of 5.5–102 m. The IV grade surrounding rock is 2560 m long and the V grade surrounding rock is 4222.45 m long. The tunnel longitudinal and cross-section drawings are shown in Figure 1. The geological strata in the tunnel site area are mainly composed of Quaternary Middle Pleistocene aeolian clay loess, mainly hard plastic, with developed vertical joints. The section of the tunnel body passes through shallow buried slow slopes, hard plastic loess, and underground water-affected sections, which pose high construction risks and safety risks. The main type of groundwater in the Shangge Village Tunnel is pore water in the Quaternary loose layer, which is mainly distributed in the upper part of the loess plateau. The aquifer is mainly the middle Pleistocene loess. The loess layer has both the general characteristics of loose layer pore water and the hydraulic properties of fissure water. The particles in this layer are coarse, the structure is loose, and the porosity is high. It is the main aquifer in the loess plateau area, as well as a storage space and transport channel for groundwater. The groundwater level line is located above the tunnel body and is deeply controlled by factors such as rainfall, the size of the loess plateau, terrain cutting, and the thickness of the loess layer. According to drilling data and the investigation of water wells in the loess plateau area, the groundwater level is buried at a depth of about 50–70 m, and the thickness of the aquifer is 10–30 m within the exploration depth. The area of the loess plateau where the tunnel passes through is complete and open, and the groundwater storage conditions in the center of the loess plateau are relatively good, with a shallow water level burial depth. In areas with deep valley cutting, the discharge conditions of the surface water and groundwater are good, while the storage conditions of the groundwater are relatively poor.

During the excavation process of the Shangge Village Tunnel on the Yinxi Railway (the Ganning section), the surface of the initial support structure was damp, and water seepage was more severe, flowing out in drops or lines. In some sections, water flowed out in streams along the pipe shed drilling. The arch foot softened severely, the arch settlement was greater, and the local sections had more severe falling blocks, resulting in the significant deformation of the palm surface. Moreover, during the excavation of shallow buried sections, cracks appeared to varying degrees on both sides of the surface along the direction of the tunnel. At the same time, circumferential cracks appeared in the initial support-lining structure, with significant settlement of the arch crown and several sudden instability disasters leading to collapse. The disaster situation of the initial support structure is shown in Figure 2. If the water content of loess is high, it will significantly increase the probability of construction risks such as large deformation, falling blocks, and collapse during construction. As the tunnel excavation progresses, the water content of the excavation section also changes. In addition, after excavation, the water content will further increase due to the relaxation of the unloading surrounding rock.

(a)

(b)
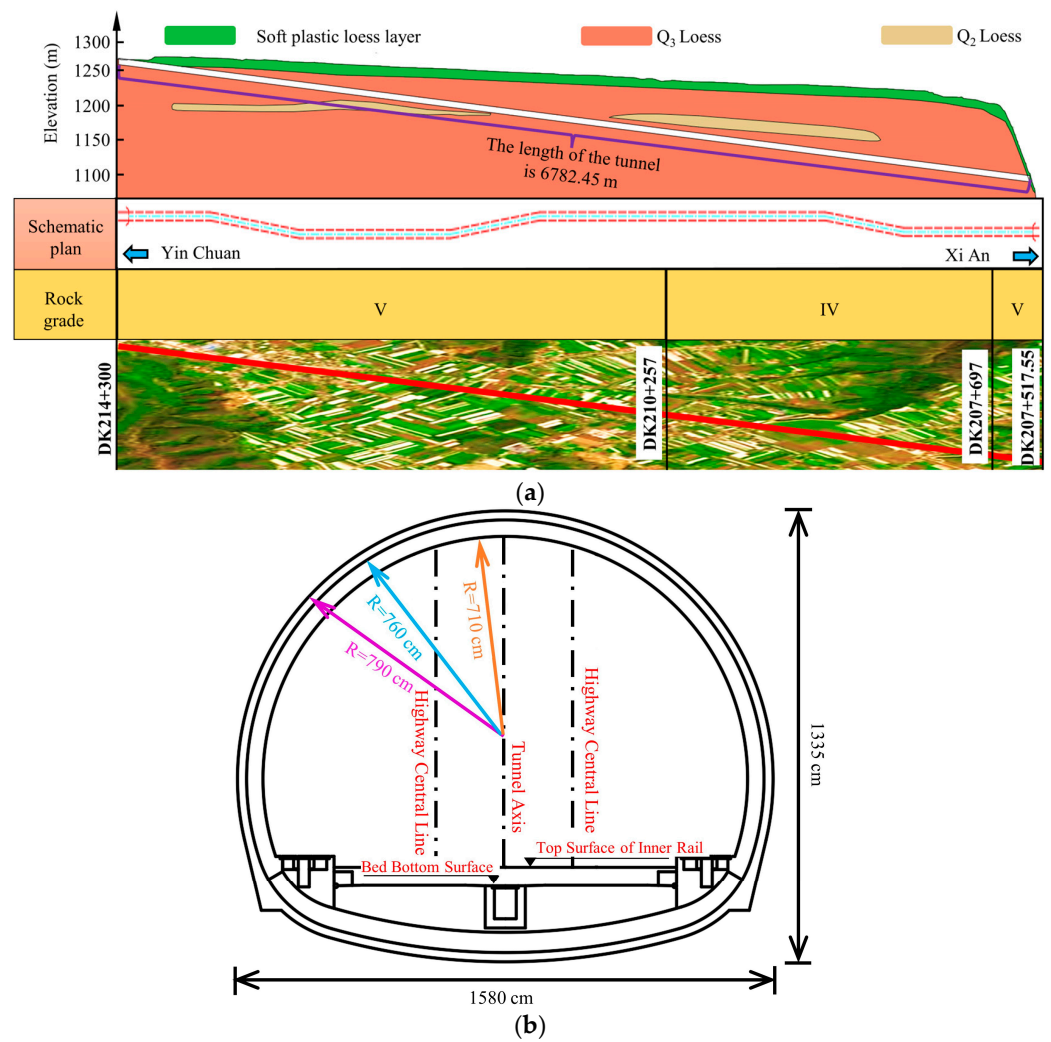
Figure 1. Tunnel longitudinal and cross-section drawings. (**a**) Longitudinal section (Q2: Mediopleistocene; Q3: Late Pleistocene); (**b**) cross-section.

(a)

(b)
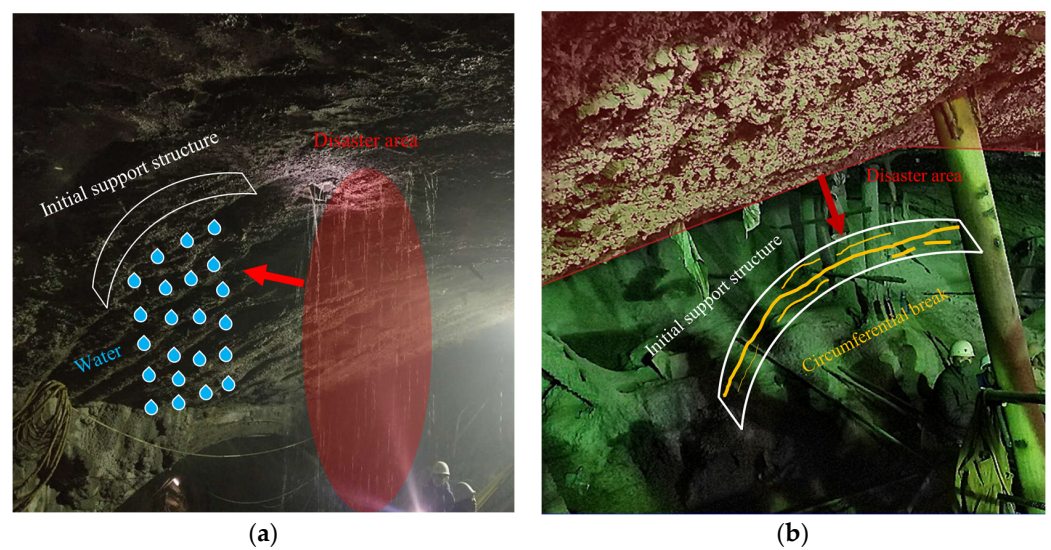
Figure 2. Preliminary support-structure-disaster schematic diagram. (**a**) Initial support structure seepage disaster; (**b**) initial support structure deformation disaster.

3. Physical and Mechanical Properties of Loess

In order to reduce the disturbance to undisturbed soil samples, after sampling the loess surrounding rock on site, immediately seal the samples with preservative film, wrap the samples with damping foam, and send them to the laboratory for physical and mechanical tests within 24 h. The physical and mechanical parameters of the loess sample obtained through statistical analysis are shown in Figure 3. The range of the water content of the loess samples in this test is 22~30.5%. The weight of loess increases with the increase in the moisture content, but the growth rate changes with a trend of "increase-decrease-increase-decrease-increase". The Poisson's ratio of loess is positively correlated with its water content, with a growth rate of 34.4%. The elastic modulus, internal friction angle, and cohesion of loess decrease with the increase in the water content, and the degradation of the internal friction angle is very significant, decaying from 35.0 kPa to 2.15 kPa; the attenuation amplitude of internal friction is relatively small, only decreasing by 18.3%. When the water content ranges from 27.4% to 29.5%, there is a rate change zone in the elastic modulus, internal friction angle, and cohesion. The attenuation rate of the internal friction angle increases, while the attenuation rate of the elastic modulus and cohesion decreases. However, the rate change is small, and there is no obvious step in the curve. As the water content of loess increases, water molecules will form a lubricating layer between loess particles, reducing the contact area and internal friction angle between particles. In addition, after absorbing water, loess will expand, leading to larger voids in the soil and reduced interaction forces between particles. The above are the main reasons for the changes in the mechanical parameters of loess. Therefore, water is an important factor affecting the deterioration of loess surrounding rock; if the water content continues to increase, the strength of the surrounding rock will also decrease synchronously.
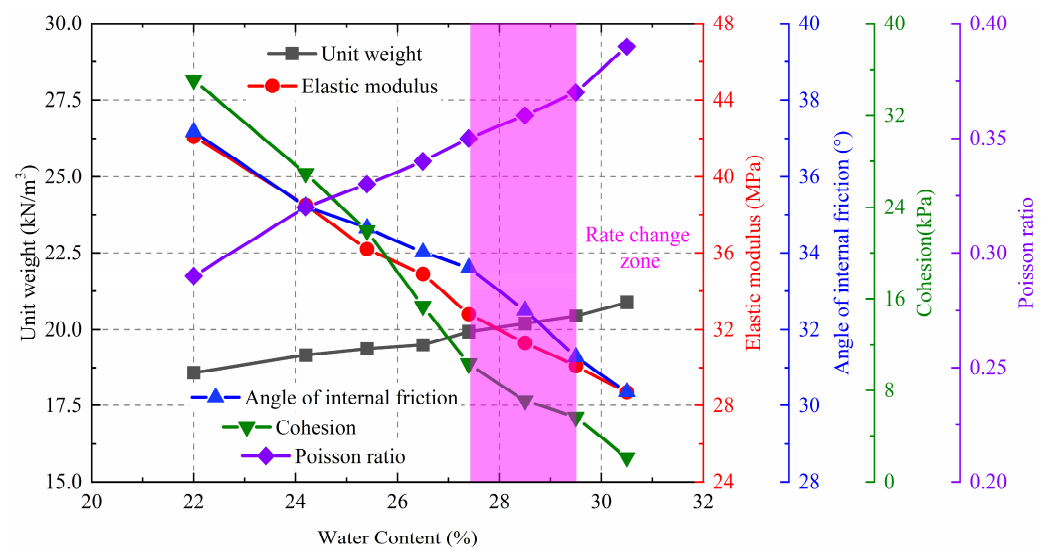
Figure 3. Physical and mechanical parameters of loess.

4. Analysis of Deformation Mechanism of Primary Support Structure

4.1. Numerical Model

This article uses FLAC 3D software to simulate the excavation and support of tunnels, with a burial depth of 64.7 m. The excavation is carried out by using the three-step reserved core geotechnical method. The excavation sequence is to first excavate the upper step, then excavate the core soil, and finally excavate the lower step. The excavation cycle footage is 2 m/d. The model stipulates that the direction of the longitudinal mileage increase along the tunnel is in the X-direction, the vertical direction is in the Z axis direction, and the centerline of the tunnel excavation cross-section is in the positive direction of the Y axis to the right. According to the Saint Venant principle, in order to reduce the influence of boundary effects on tunnel construction, the distance between the tunnel and the model

boundary is 3–5 times the diameter of the excavated hole, and the model has a size of 100 m in the X-, Y-, and Z-directions 100 m × 100 m × 100 m. The boundary conditions are displacement constraints, with Y-direction constraints applied to the left and right sides of the model, X-direction constraints applied to the front and rear boundaries, Z-direction constraints applied to the bottom surface, and a free boundary applied to the upper boundary. Set up vault-settlement monitoring points (GD01) and sidewall-convergence monitoring points (SL02 and SL03) inside the tunnel. The whole tunnel model and its excavation and measuring point layout diagram are shown in Figure 4.
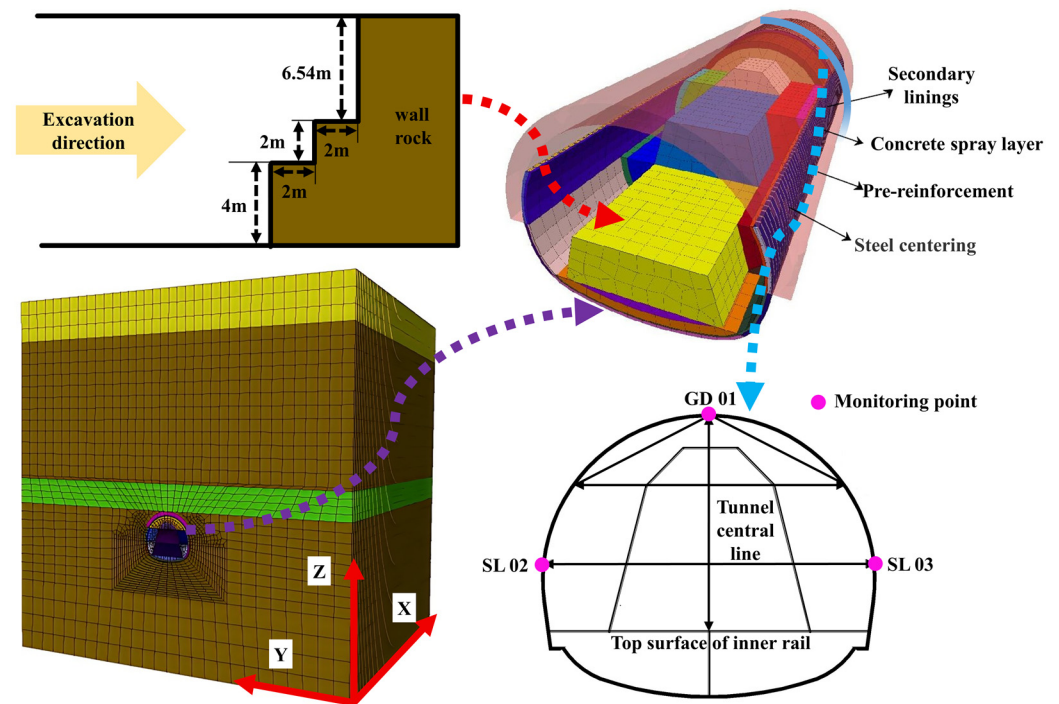
Figure 4. The whole tunnel model and its excavation and measuring point layout diagram.

The surrounding rock was analyzed by using the Mohr–Coulomb constitutive model [3] with eight different water contents in the surrounding rocks. The detailed mechanical parameters are shown in Figure 3. The lining structure adopts an elastic model [24], among which the initial support structure adopts C30 concrete with a thickness of 30 cm. The secondary lining structure adopts C40 concrete with a thickness of 50 cm [41], and its mechanical parameters are shown in Table 1.

Table 1. Mechanical property parameters of support.

Supporting Structure	Unit Weight (kN/m^3)	Elastic Modulus (MPa)	Poisson Ratio	Thickness (cm)
Initial support structure	22	25,000	0.25	30
Secondary lining	25	32,000	0.25	50

4.2. Results

4.2.1. Settlement

According to the analysis of the numerical simulation results, it can be seen that the relationship between the excavation distance and settlement under different water contents is shown in Figure 5. When the distance between the monitoring point and the palm surface is constant, as the water content increases, the settlement of the vault also increases synchronously, and the settlement rate shows a trend of first increasing and then decreasing. During the process of increasing the distance between the monitoring point and

the palm face from 0 m to 30 m, the settlement of the surrounding rock increased sharply, with the largest increase in settlement reaching 187 mm when the water content of the surrounding rock was 30.5%. As the distance between the monitoring point and the palm surface increases from 30 m to 40 m, the settlement rate of the surrounding rock begins to decrease. The smaller the water content of the surrounding rock, the earlier the settlement tends to stabilize. The settlement rate of the surrounding rock with a water content of 22.0% is the smallest, only 0.6 mm/d. When the distance between the monitoring point and the palm surface is 40–60 m, the settlement under various working conditions tends to be constant. As the excavation distance increases, there are three stages of rapid growth, slow growth, and stable deformation of the vault settlement; the lower the water content of the surrounding rock, the earlier the settlement of the vault enters the stable stage. Therefore, a lower water content in the surrounding rock is beneficial for controlling the settlement of the vault.
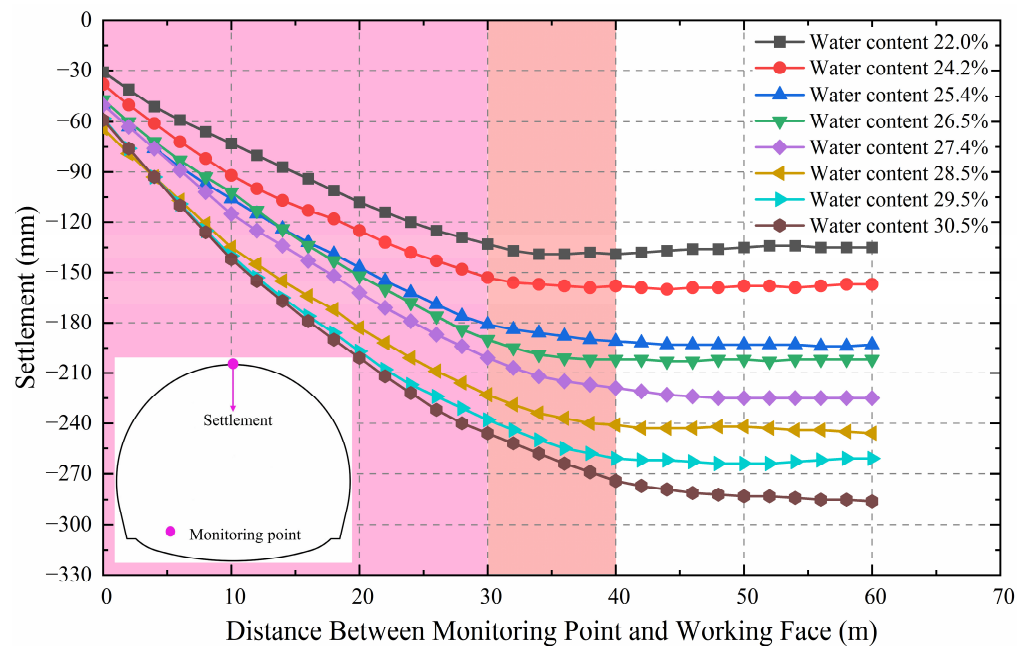
Figure 5. The relationship between excavation distance and settlement under different water content.

4.2.2. Convergence

According to the analysis of the numerical simulation results, it can be seen that the relationship between the excavation distance and convergence under different water contents is shown in Figure 6. When the distance between the monitoring point and the palm surface is constant, the convergence of the sidewall increases with the increase in the water content. The convergence rate of the sidewall and the settlement rate of the arch show a trend of first increasing and then decreasing. In addition, as the excavation distance increases, the convergence of the sidewall undergoes three stages: rapid growth, slow growth, and stable stability. When the distance between the monitoring point and the palm face is 0–40 m, the convergence is in a rapid growth stage, and the deformation of the surrounding rock with a water content of 30.5% is the largest, reaching 184 mm. When the distance between the monitoring point and the palm face is between 40 and 50 m, the convergence is in a slow growth stage, and the deformation decreases with the decrease in the surrounding rock water content. When the distance between the monitoring point and the palm face is greater than 50 m, the convergence begins to enter a stable and unchanging stage. The lower the water content of the surrounding rock, the earlier the time to enter the stable stage. Among them, the convergence of the sidewall with a water content of 22.0% of the surrounding rock enters the stable stage first when it is 50 m away from the palm face.
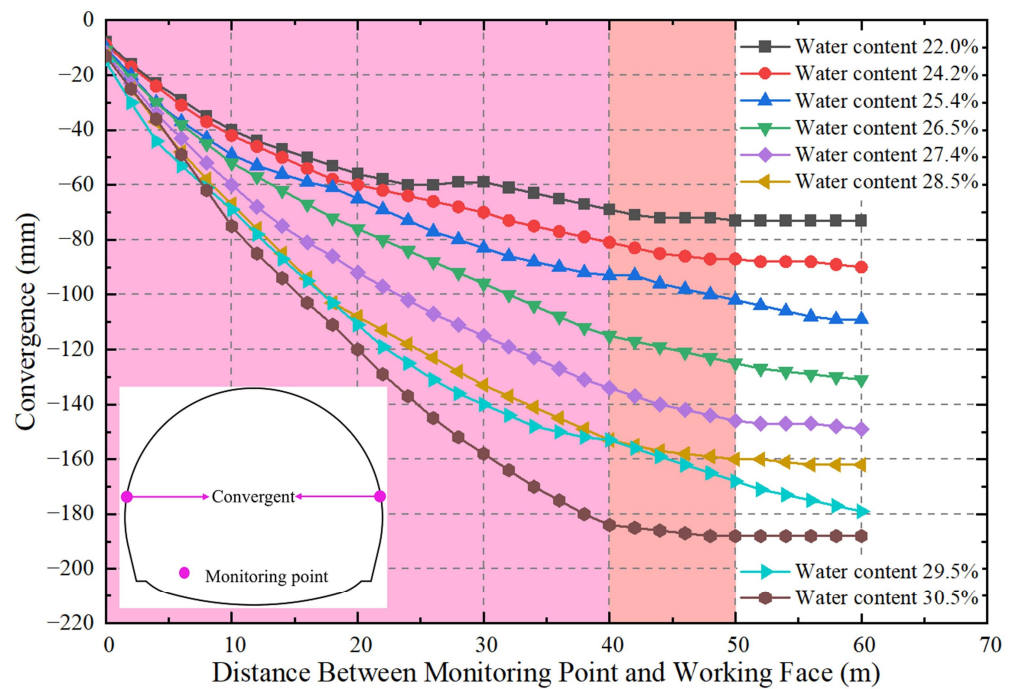
Figure 6. The relationship between excavation distance and convergence under different water contents.

4.3. Discussion

Water molecules play a lubricating role in soil, reducing the cohesion inside the soil. When the water content increases, water molecules fill the gaps between soil particles, reducing the contact area between particles and thereby reducing the friction and cohesion between particles. This leads to a decrease in the overall strength of the surrounding rock, making it more susceptible to excavation disturbances, which in turn leads to an increase in vault settlement and sidewall convergence. At the same time, the presence of water molecules can also change the pore structure of the soil, increase the porosity of the soil, and further reduce the strength of the surrounding rock. Therefore, as the water content increases, the strength of the surrounding rock decreases, leading to the increased settlement of the vault and convergence of the sidewalls. In addition, more seepage channels in the soil are interconnected, and the influence of excavation disturbances on the surrounding rock is expanded, which leads to an increase in the vault settlement and sidewall convergence.

The lower the water content of the loess surrounding rock, the lower the settlement of the vault and the convergence of the sidewall of the surrounding rock; however, the lower the water content of the loess surrounding rock, the better. If the water content is too low, it will damage the ecological environment. Therefore, the water content of the loess surrounding rock should not only be suitable for the ecological environment of the Shangge Village Tunnel but also be conducive to controlling the deformation of the initial support structure of the tunnel. This water content is called the water content threshold. According to on-site geological survey data, the surface of the Shangge Village Tunnel is distributed in villages, and some sections have orchards. If the water content of the loess is excessively reduced, it will damage the ecological environment of the orchards; therefore, it is necessary to select a moisture threshold from the actual water content dataset of on-site soil samples. Indoor experiments have measured that the on-site soil samples have eight water contents, which are 22.0%, 24.2%, 25.4%, 26.5%, 27.4%, 28.5%, 29.5%, and 30.5%. Therefore, 22.0% is selected as the water content threshold for the Shangge Village Tunnel. In addition, the net clearance of this tunnel is 13.38 m. According to Code 8.5.5 [42] of the Technical Code for Railway Tunnel in Loess (Q/CR 9511-2014), the limit value of the arch settlement is 180.63–254.22 mm.

When the settlement value of the vault is 180.63 mm, the water content of the loess is 24.95%. Because 22% is less than 24.95%, it is reasonable to choose 22.0% as the water content threshold for the Shangge Village Tunnel.

5. Treatment Measure

5.1. Surface Precipitation

5.1.1. Design Scheme

During on-site construction, the surface precipitation well scheme is used to control the water content of the surrounding rock in the DK 208+560-DK 208+660 section of the Shangge Village Tunnel. The surface precipitation wells are symmetrically arranged on both sides of the tunnel (as shown in Figure 7), located 9 m outside the tunnel contour line and 20 m away from the same side wells. A total of 12 precipitation wells are set up. The diameter of the precipitation well is 0.325 m and the burial depth is 120 m. The casing length of the well tube is 80 m, the filter tube length is 36 m, and the lower sand settling tube length is 6 m. The filter tube section is wrapped with 80 mesh steel wire mesh. We backfill gravel as a filter layer, with a gravel thickness of approximately 20 cm and a gravel gradation of 10–20 mm. After drilling is completed, immediately lower the well pipe; backfill the filter layer; and clean the precipitation well until the water is clear, the sand is clean, and there is no sediment.
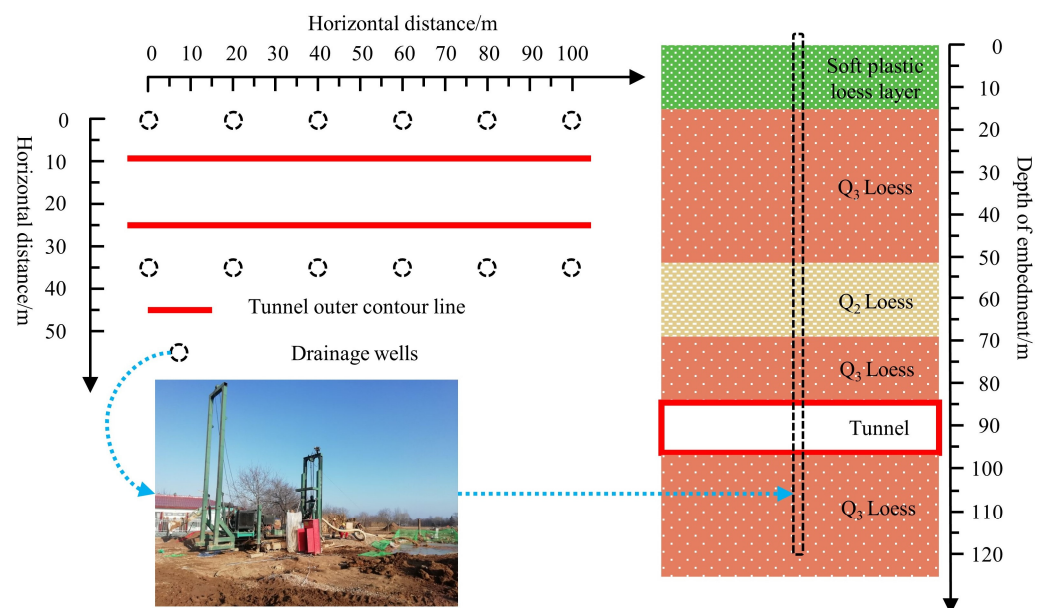
Figure 7. Layout diagram of surface precipitation well.

5.1.2. Results and Analyses

Two monitoring wells are set up at the tunnel construction site to obtain the water content of the strata at different burial depths. The G1 monitoring well is located in the area without surface precipitation, and the G2 monitoring well is located in the area with surface precipitation. The burial depth of the monitoring well should be consistent with that of the surface precipitation well. The distribution of the water content in the loess strata before and after surface precipitation is shown in Figure 8. Before taking the surface precipitation well measures, the maximum and minimum water content in the formation were 35.21% and 11.26%, respectively, with an average water content of 25.77%. After adopting the surface precipitation well measures, the maximum water content in the formation is 23.34%, the minimum water content is 11.78%, and the average water content in the formation is 19.92%. When the depth range below the surface is about 0–30 m, the degree of influence of the surface water vapor evaporation is deeper, resulting in larger water content in the strata with a depth of 0–120 m before and after the implementation of the surface precipitation

well measures. Therefore, the analysis should be based on the water content of the strata with a burial depth of 30–120 m. Before surface precipitation, the average water content of the strata with a burial depth of 30–120 m was 31.03%; after surface precipitation, the average water content of the strata with a burial depth of 30–120 m was 21.81%, which is close to the threshold of the water content. From this, it can be seen that the surface precipitation well scheme can meet the requirements of water content control.
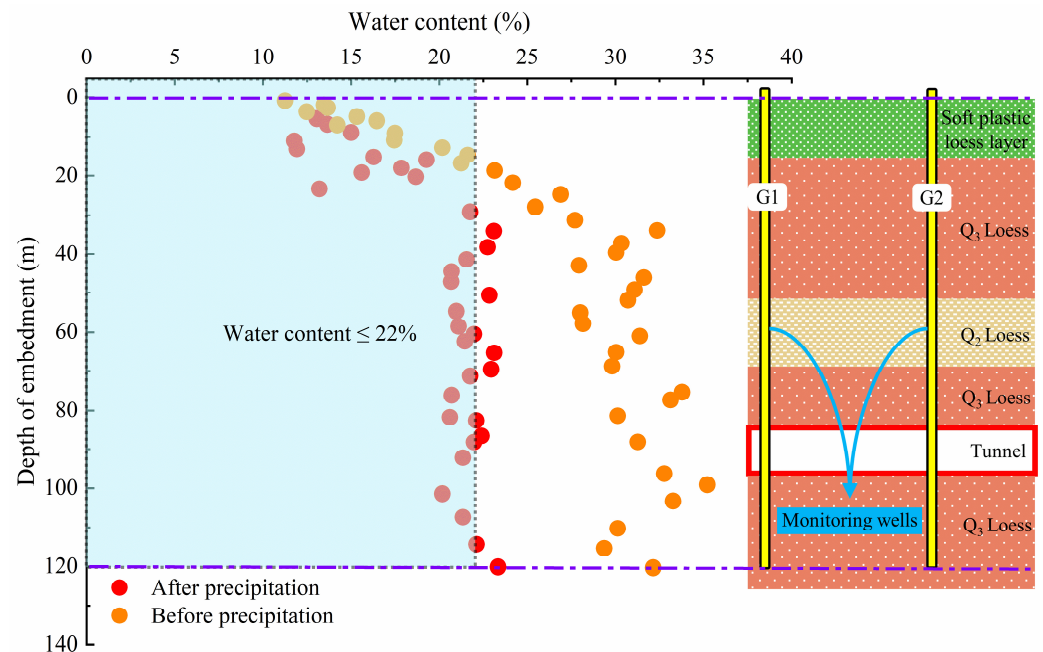
Figure 8. The change in water content in loess strata before and after precipitation.

5.2. Curtain Grouting

5.2.1. Design Scheme

Firstly, the water content of the surrounding rock around the tunnel is adjusted to around 22% through surface precipitation. Secondly, the grouting parameters were adjusted, as shown in Table 2. Finally, the surrounding rock behind the palm face was reinforced by curtain grouting, as shown in Figure 9. To prevent grout and fissure water from gushing out from the grouting face and to ensure the expected quality of grouting, it is necessary to set up a C30 concrete grout stop wall with a thickness of 2 m on the grouting face between the initial support structure and the temporary inverted arch structure. The grouting material is ordinary Portland cement (P.O.42.5) with a slurry ratio of W: C=0.8:1. The length of grouting toward the back of the palm is 25 m, with a forward segmented grouting method used for 0–10 m and a sleeve valve tube bundle grouting method used for 10–25 m. The radial reinforcement range of grouting is 5 m above the initial support structure and 1.3 m below the bottom of the grout stop wall. A total of 54 grouting holes are set on the upper section of the palm face, including 15 Class A grouting holes, 12 Class B grouting holes, 15 Class C grouting holes, and 12 Class D grouting holes.

Table 2. Detailed grouting parameters.

Type	Parameter Value
Grouting diffusion radius	2 m
Injection pressure	3–5 MPa
Grouting aperture	90 mm
Injection into orbit rate	10–100 L/min
Number of grouting holes	54
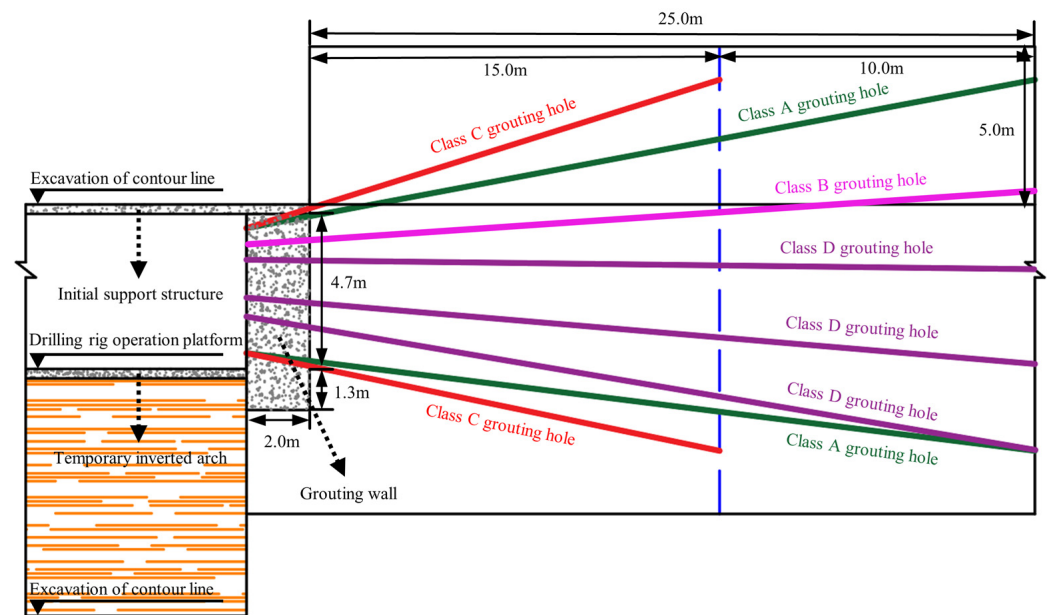
Figure 9. Curtain grouting construction schematic diagram.

5.2.2. Results and Analyses

We conducted deformation monitoring on three tunnel sections at the construction site for 30 days. Surface precipitation measures and curtain grouting measures were not taken from the DK208+570 section. Surface precipitation measures were not taken from the DK207+710 section; only curtain grouting measures were taken. For the DK208+630 section, we adopted dual measures of surface precipitation and curtain grouting. The settlement and convergence of the three monitoring sections are shown in Figure 10. The settlement of section DK208+570 reaches its maximum deformation rate from 0 to 15 days after excavation, reaching 7.78 mm/d. During the period of 15 to 30 days, the settlement begins to stabilize and eventually reaches approximately 118.74 mm. The convergence has the highest deformation rate from 0 to 13 days after excavation, reaching 4.56 mm/d. During the period of 13 to 30 days, the convergence begins to stabilize and eventually reaches about 60.14 mm. For the DK207+710 section, we adopted curtain grouting measures based on the DK208+570 section, reducing settlement by about 17.69% and convergence by about 11.86%. After adjusting the water content of the surrounding rock around section DK208+630 to about 22% through surface precipitation measures, curtain grouting reinforcement measures were carried out. The settlement of section DK208+630 ultimately stabilizes at around 73.88 mm, which is about 37.29% lower than that of section DK208+570 and about 23.81% lower than that of section DK207+710. The maximum convergence of section DK208+630 reaches 39.54 mm, which is about 34.26% and 25.41% lower than that of section DK208+570 and section DK207+710, respectively.

According to the Technical Code for Railway Tunnel Loess (Q/CR 9511-2014) [42] and Technical Code for Monitoring Measurement of Railway Tunnel (Q/CR 9218-2015) [43], the range of the cumulative deformation yellow warning values is determined to be 75–150 mm. If the deformation value of the tunnel section reaches the yellow warning value range, it indicates that the initial support structure of the tunnel is in an unstable state and may be damaged at any time. According to Figure 10, the settlement of section DK208+570 is within the range of yellow warning deformation values. Although the settlement value of section DK207+710 decreased compared to section DK208+570, it is still within the yellow warning deformation value range, and there is a risk of damage to the initial support structure. The settlement and convergence of section DK208+630 are both less than 75 mm, meeting the specification requirements [42,43]. Therefore, the combination of surface precipitation measures and curtain grouting measures can ensure the safe construction of loess tunnels.
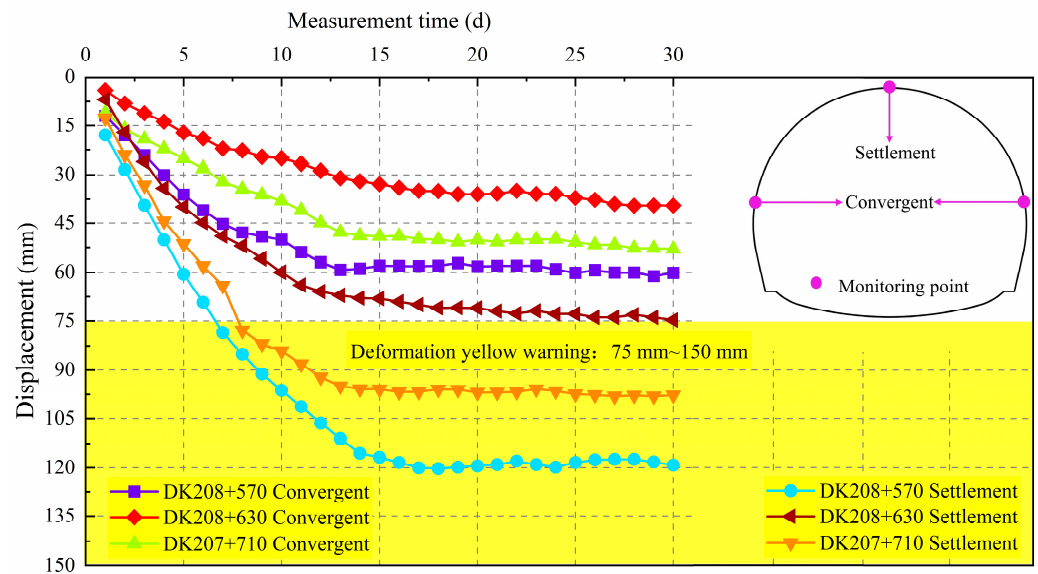
Figure 10. Deformation monitoring timescale after curtain grouting reinforcement measures—curve chart.

6. Discussion

In soil, the presence of water molecules has a significant effect on its mechanical properties. With the increase in the water content, water molecules fill the gap between soil particles and reduce the contact area between particles, thus deteriorating the mechanical parameters of loess and reducing the overall strength of the soil. At the same time, the presence of water molecules also changes the pore structure of the soil and further reduces the strength of the soil. In addition, more seepage channels in the soil are connected to each other, which expands the influence range of the soil. Therefore, the lower water content of loess is more conducive to the stability of the surrounding rock. However, adjusting the water content of the surrounding rock too low by precipitation measures not only destroys the ecological environment but also makes it easier for water molecules in the surrounding high-moisture loess strata to reincrease the water content of the surrounding rock through the seepage channel [44,45]. In summary, this article proposes a water content threshold and reinforces the loess surrounding rock on the basis of the water content threshold.

The flow chart of the loess tunnel reinforcement is shown in Figure 11. Firstly, the mechanical parameters of loess are obtained through indoor physical and mechanical tests. Secondly, based on the ecological environment where the loess tunnel is located, the water content threshold is determined to be 22% in order to avoid economic and environmental losses caused by excessive precipitation and grouting. Then, through surface precipitation measures, the water content of the surrounding rock around the tunnel is reduced to be around the water content threshold, thereby improving the shear strength, compressive strength, and enhancing the ability of the surrounding rock to resist disturbance. Finally, curtain grouting reinforcement measures are adopted to further improve the overall stability and bearing capacity of the surrounding rock. The reinforcement scheme proposed in this article can effectively ensure the construction and operation safety of loess tunnels. According to the on-site monitoring data of the Shanghai Village Tunnel, our proposed rock reinforcement scheme effectively controls the settlement of the tunnel vault and the convergence of the sidewalls while meeting the requirements of the ecological environment, thereby improving the safety and stability of the project. This study mainly focuses on the ecological environment and regulatory requirements of the Shangge Village Tunnel to determine the threshold of the surrounding rock water content. But in other loess tunnels, there may be other factors to consider, such as construction convenience, engineering economy, etc. Therefore, it is necessary to combine more practical engineering cases and summarize more systematic methods to determine the threshold of the loess water content. In addition, this article has not conducted an in-depth exploration of the research of curtain

grouting materials. However, future research can consider using more advanced and superior new materials.
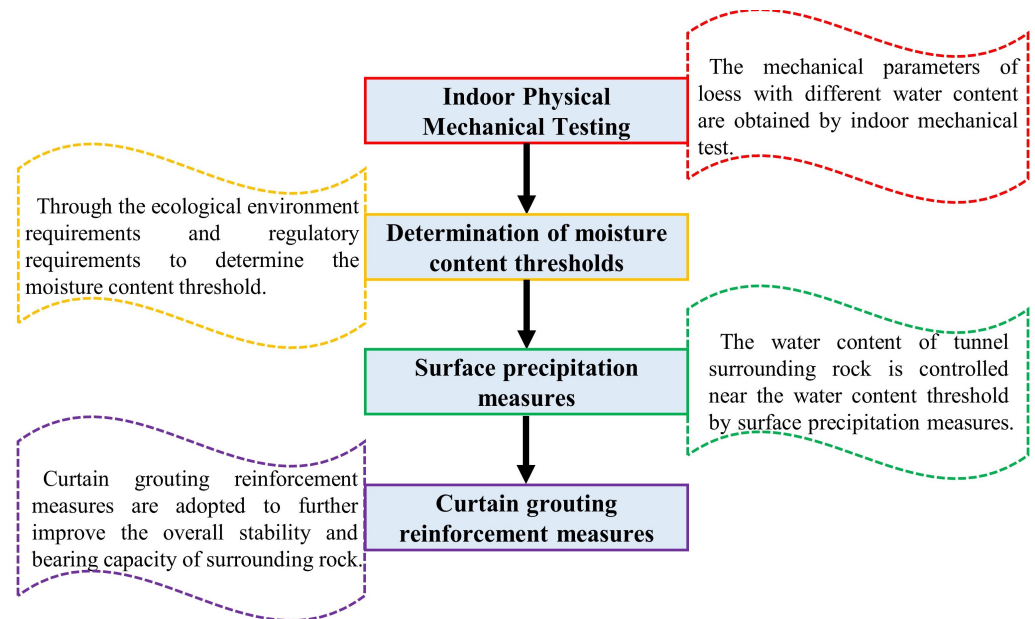
Figure 11. Flow chart of loess tunnel reinforcement.

7. Conclusions

(1) As the water content of loess increases, water molecules will form a lubricating layer between loess particles, reducing the contact area and internal friction angle between particles. At the same time, after absorbing water, loess will expand, causing the voids in the soil to become larger and the interaction forces between particles to decrease. Therefore, during the construction process of loess tunnels, the water content of the surrounding rock increases, which reduces the cohesion, internal friction angle, and elastic modulus of the surrounding rock, leading to the deterioration of the strength of the surrounding rock, making it more sensitive to subsequent excavation disturbances, and ultimately causing damage to the initial support structure.

(2) As the water content of the loess surrounding rock increases, the settlement of the vault and the convergence of the sidewalls of the surrounding rock show an increasing trend. In addition, the settlement of the vault undergoes three stages: rapid growth, slow growth, and stable stability within the range of 0~30 m, 30~40 m, and 40~60 m from the monitoring section to the palm surface, respectively. The convergence of the sidewalls occurs within the range of 0~40 m, 40~50 m, and 50~60 m from the monitoring section to the palm surface, exhibiting rapid growth, slow growth, and stable stages, respectively. It is worth noting that compared to the vault settlement of the surrounding rock, the convergence of the sidewalls has a significant lag.

(3) Based on the deformation mechanism of the initial support structure of the Shangge Village Tunnel and the requirements of the ecological environment, a water content threshold of 22% is set for the surrounding rock. Based on this threshold, a rock reinforcement scheme combining surface precipitation and curtain grouting is adopted. By taking these measures, the settlement of the vault and the convergence of the sidewalls are both lower than the yellow warning deformation value. Compared with unreinforced and single-curtain grouting measures, the settlement of the vault decreased by 37.29% and 23.81% respectively, and the convergence of the sidewalls decreased by 34.26% and 25.1%, respectively. This indicates that adopting a combination of surface precipitation and curtain grouting for surrounding rock reinforcement has a significant effect on reducing the settlement of the vault and the convergence of the sidewalls.

(4) The reinforcement scheme for loess tunnels based on the water content threshold is analyzed through on-site monitoring data, which prove that this reinforcement scheme can effectively reduce vault settlement and sidewall convergence, ensuring the safety of tunnel construction and operation periods. Therefore, similar studies in the future can further propose more systematic methods to determine more accurate water content thresholds from the aspects of construction convenience and the engineering economy based on this study and try different reinforcement measures to provide more scientific technical support for the construction and operation of loess tunnels.

References

1. Xu, Z.; Cai, N.; Li, X.; Xian, M.; Dong, T. Risk Assessment of Loess Tunnel Collapse during Construction Based on an Attribute Recognition Model. *Bull. Eng. Geol. Environ.* **2021**, *80*, 6205–6220. [CrossRef]
2. Fu, J.; Li, H.; Zhu, K.; Chen, Y.; Lei, Z. Study on Expansion Characteristics and Expansion Potential of Gypsum Rock. *Geofluids* **2022**, *2022*, 6921150. [CrossRef]
3. Li, H.; Fu, J.; Chen, B.; Zhang, X.; Zhang, Z.; Lang, L. Mechanical Properties of GFRP Bolts and Its Application in Tunnel Face Reinforcement. *Materials* **2023**, *16*, 2193. [CrossRef]
4. Sharifzadeh, M.; Daraei, R.; Broojerdi, M.S. Design of Sequential Excavation Tunneling in Weak Rocks through Findings Obtained from Displacements Based Back Analysis. *Tunn. Undergr. Space Technol.* **2012**, *28*, 10–17. [CrossRef]
5. Daraei, A.; Zare, S. A New Multi-Graph Approach for Selecting the Sequential Excavation Method of Civil Tunnels. *Tunn. Undergr. Space Technol.* **2019**, *91*, 102999. [CrossRef]
6. Wang, M.; Dong, Y.; Yu, L. Analytical Solution for a Loess Tunnel Based on a Bilinear Strength Criterion. *Soil. Mech. Found. Eng.* **2020**, *57*, 296–304. [CrossRef]
7. Yates, K.; Fenton, C.H.; Bell, D.H. A Review of the Geotechnical Characteristics of Loess and Loess-Derived Soils from Canterbury, South Island, New Zealand. *Eng. Geol.* **2018**, *236*, 11–21. [CrossRef]
8. Yusoff, I.N.; Mohamad Ismail, M.A.; Tobe, H.; Miyoshi, T.; Date, K.; Yokota, Y. Discontinuity Pattern Detection and Orientation Measurement for Tunnel Faces by Using Structure from Motion Photogrammetry. *Displays* **2023**, *76*, 102356. [CrossRef]
9. Ali, A.; Achyuthan, H. Paleoenvironment Shifts during MIS 3: Loess and Loess Paleosols of Kashmir Valley, India. *J. Earth Syst. Sci.* **2020**, *129*, 177. [CrossRef]
10. Goossens, D. Scale Model Simulations of the Deposition of Loess in Hilly Terrain. *Earth Surf. Processes Landf.* **1988**, *13*, 533–544. [CrossRef]
11. Hong, Q.; Lai, H.; Liu, Y.; Chen, R. Distress Mechanism and Treatment Measures in Construction of Large Cross-Section Tunnel Passing through Q2 Soft-Plastic Loess Layer. *Bull. Eng. Geol. Environ.* **2023**, *82*, 165. [CrossRef]
12. Wu, J.; Jiang, J.; Li, Z.; Yang, Y.; Hou, Z.; Sun, Z.; Gong, X. Stability Analysis Method for Initial Support Structure of Tunnel in Swelling Loess. *Processes* **2023**, *11*, 1090. [CrossRef]
13. Wang, Z.; Cai, Y.; Xie, Y.; Zhang, M.; Lai, J.; Qiu, J.; Liu, T. Laboratory Study on Mechanical Behavior of Hollow π-Type Steel–Concrete Composite Support in Loess Tunnel. *Tunn. Undergr. Space Technol.* **2023**, *141*, 105280. [CrossRef]
14. Zhang, X.; Du, D.; Man, T.; Ge, Z.; Herbert, E. Huppert Particle Clogging Mechanisms in Hyporheic Exchange with Coupled Lattice Boltzmann Discrete Element Simulations. *Phys. Fluids* **2024**, *36*, 013312. [CrossRef]
15. Liang, Q.; Li, J.; Wu, X.; Zhou, A. Anisotropy of Q2 Loess in the Baijiapo Tunnel on the Lanyu Railway, China. *Bull. Eng. Geol. Environ.* **2016**, *75*, 109–124. [CrossRef]

16. Shi, W.; Qiu, J.; Zhang, C.; Wang, Q.; Lai, J.; Li, B.; Mao, Z. Immersion Mode and Spatiotemporal Distribution Characteristic of Water Migration in Loess Tunnel. *Arab. J. Geosci.* **2022**, *15*, 654. [CrossRef]

17. Li, Z.-W.; Huang, C.-Y.; Wang, H.-X.; Xing, S.-C.; Long, M.-C.; Liu, Y. Determination of Heat Transfer Representative Element Volume and Three-Dimensional Thermal Conductivity Tensor of Fractured Rock Masses. *Int. J. Rock Mech. Min. Sci.* **2023**, *170*, 105528. [CrossRef]

18. Song, W.; Lai, H.; Liu, Y.; Yang, W.; Zhu, Z. Field and Laboratory Study of Cracking and Safety of Secondary Lining for an Existing Highway Tunnel in Loess Ground. *Tunn. Undergr. Space Technol.* **2019**, *88*, 35–46. [CrossRef]

19. Liu, Y.; Lai, H.; Xie, Y.; Song, W. Cracks Analysis of Highway Tunnel Lining in Flooded Loess. *Proc. Inst. Civ. Eng. Geotech. Eng.* **2017**, *170*, 62–72. [CrossRef]

20. Wang, D.; Zhao, X.; Qiu, C.; Guo, X.; Du, Y.; Li, X.; Gao, Y.; Xuan, J. Experimental and Numerical Investigation on the Damage Mechanism of a Loess–Mudstone Tunnel in Cold Regions. *Atmosphere* **2023**, *14*, 1391. [CrossRef]

21. Li, R.; Bai, W.; Li, R.; Jiang, J. Study on Stress and Displacement of Axisymmetric Circular Loess Tunnel Surrounding Rock Based on Joint Strength. *Appl. Sci.* **2023**, *13*, 6836. [CrossRef]

22. Li, X.; Wang, L.; Hong, B.; Li, L.; Liu, J.; Lei, H. Erosion Characteristics of Loess Tunnels on the Loess Plateau: A Field Investigation and Experimental Study. *Earth Surf. Process. Landforms* **2020**, *45*, 1945–1958. [CrossRef]

23. Qiu, J.; Liu, D.; Zhao, K.; Lai, J.; Wang, X.; Wang, Z.; Liu, T. Influence Spatial Behavior of Surface Cracks and Prospects for Prevention Methods in Shallow Loess Tunnels in China. *Tunn. Undergr. Space Technol.* **2024**, *143*, 105453. [CrossRef]

24. Hong, Q.; Lai, H.; Liu, Y.; Ma, X.; Xie, J. Deformation Control Method of a Large Cross-Section Tunnel Overlaid by a Soft-Plastic Loess Layer: A Case Study. *Bull. Eng. Geol. Environ.* **2021**, *80*, 4717–4730. [CrossRef]

25. Liang, Q.-G.; Wang, L.; Li, D.-W. Study on the Classification of Loess Ground in Tunnel Engineering. In *IACGE 2013: Challenges and Recent Advances in Geotechnical and Seismic Research and Practices*; American Society of Civil Engineers: Chengdu, China, 2013; pp. 79–87.

26. Cheng, X.; Feng, H.; Qi, S.; Zhang, X.; Liu, B. Dynamic Response of Curved Wall LTSLS Under the Interaction of Rainwater Seepage and Earthquake. *Geotech. Geol. Eng.* **2017**, *35*, 903–914. [CrossRef]

27. Xue, X.; Xie, Y.; Zhou, X. Study on the Life-Cycle Health Monitoring Technology of Water-Rich Loess Tunnel. *Adv. Mater. Sci. Eng.* **2019**, *2019*, 9461890. [CrossRef]

28. Weng, X.; Sun, Y.; Zhang, Y.; Niu, H.; Liu, X.; Dong, Y. Physical Modeling of Wetting-Induced Collapse of Shield Tunneling in Loess Strata. *Tunn. Undergr. Space Technol.* **2019**, *90*, 208–219. [CrossRef]

29. Baker, E.A.; Manenti, S.; Reali, A.; Sangalli, G.; Tamellini, L.; Todeschini, S. Combining Noisy Well Data and Expert Knowledge in a Bayesian Calibration of a Flow Model under Uncertainties: An Application to Solute Transport in the Ticino Basin. *Int. J. Geomath.* **2023**, *14*, 8. [CrossRef]

30. Seifi, A.; Ehteram, M.; Singh, V.P.; Mosavi, A. Modeling and Uncertainty Analysis of Groundwater Level Using Six Evolutionary Optimization Algorithms Hybridized with ANFIS, SVM, and ANN. *Sustainability* **2020**, *12*, 4023. [CrossRef]

31. Li, Q.; Liu, M.; Yu, Y. Mechanical Behavior of Loess Tunnels Caused by Surface Water Joints Infiltration. *Adv. Civ. Eng.* **2022**, *2022*, 3056668. [CrossRef]

32. Yan, Q.; Li, Y.; Yuan, Y. Research on the Evolution Mechanism of Large Deformation of Expansive Loess Tunnel under Rainfall. *Math. Probl. Eng.* **2022**, *2022*, 9930738. [CrossRef]

33. Hong, Q.; Lai, H.; Liu, Y. Failure Analysis and Treatments of Collapse Accidents in Loess Tunnels. *Eng. Fail. Anal.* **2023**, *145*, 107037. [CrossRef]

34. Liu, Y.; Lai, H. Experimental Study on Lining Cracking of Shallow Buried Loess Tunnel under the Simulation of Effect of Slide Surface Immersion. *Appl. Sci.* **2020**, *10*, 6080. [CrossRef]

35. Xue, Y.; Ma, X.; Yang, W.; Ma, L.; Qiu, D.; Li, Z.; Li, X.; Zhou, B. Total Deformation Prediction of the Typical Loess Tunnels. *Bull. Eng. Geol. Environ.* **2020**, *79*, 3621–3634. [CrossRef]

36. Qiu, J.; Lu, Y.; Lai, J.; Zhang, Y.; Yang, T.; Wang, K. Experimental Study on the Effect of Water Gushing on Loess Metro Tunnel. *Environ. Earth Sci.* **2020**, *79*, 261. [CrossRef]

37. Li, J.; Shao, S.; Shao, S. Collapsible Characteristics of Loess Tunnel Site and Their Effects on Tunnel Structure. *Tunn. Undergr. Space Technol.* **2019**, *83*, 509–519. [CrossRef]

38. Cui, G.; Ma, J.; Wang, D. A Large 3D Laboratory Test on the Deformation Characteristic of Shallow Loess Tunnel under Different Plastic States. *Bull. Eng. Geol. Environ.* **2021**, *80*, 7577–7590. [CrossRef]

39. Shao, S.; Shao, S.; Li, J.; Zhu, D. Collapsible Deformation Evaluation of Loess under Tunnels Tested by in Situ Sand Well Immersion Experiments. *Eng. Geol.* **2021**, *292*, 106257. [CrossRef]

40. Wei, Z.; Zhu, Y. Seepage in Water-Rich Loess Tunnel Excavating Process and Grouting Control Effect. *Geofluids* **2021**, *2021*, 5597845. [CrossRef]

41. *TB 10003-2016*; Code for Design of Railway Tunnel. China Railway Publishing House: Beijing, China, 2016.

42. *Q/CR 9511-2014*; Technical Specification for Railway Loess Tunnel. China Railway Publishing House: Beijing, China, 2016.

43. *Q/CR 9218-2015*; Technical Specification for Monitoring Measurement of Railway Tunnel. China Railway Publishing House: Beijing, China, 2015.

44. Lan, H.; Zhang, T.; Peng, J.; Zhang, F.; Li, L.; Wu, Y.; Tian, N.; Clague, J.J. Large Scale Land Reclamation and the Effects on Hydro-Mechanical Behavior in Loess and Loess-Derived Fill. *Eng. Geol.* **2023**, *323*, 107241. [CrossRef]
45. Zhao, Z.; Wang, T.; Zhang, L.; Ruan, J.; Zhu, X. Measurement and Modeling of the Evaporation Rate of Loess under High Temperature. *Int. J. Heat Mass Transf.* **2023**, *215*, 124486. [CrossRef]